Optica Applicata, Vol. XLVI, No. 4, 2016
DOI: 10.5277/oa160402

All-optical ultrafast switching in a silicon microring resonator and its application to design multiplexer/demultiplexer, adder/subtractor and comparator circuit

JAYANTA KUMAR RAKSHIT[1], JITENDRA NATH ROY[2, 3*]

[1]Department of Electronics and Instrumentation Engineering, National Institute of Technology Agartala, Tripura, India

[2]Department of Physics, National Institute of Technology Agartala, Tripura, India

[3]Department of Physics, Kazi Nazrul University, West Bengal, India

[*]Corresponding author: jnroys@yahoo.co.in

In this paper, the possibility of using a silicon waveguide based microring resonator as a nonlinear all-optical switch is described under low power operation through a two-photon absorption effect. All-optical multiplexer/demultiplexer scheme based on two cascaded microring resonators has been proposed and described. The proposed circuits require smaller number of ring resonators and a single circuit consisting of two microring resonators capable to perform both multiplexer/demultiplexer operations by simply interchanging the inputs and outputs. Two optical pump signals represented the two operands of the logical operations to modulate the two microring resonators. The demultiplexer circuit can also perform as a half-adder/subtractor and a single bit data comparator. Numerical simulation results confirming described methods are given in this paper. The performances of the schemes are analyzed by calculating the extinction ratio, contrast ratio and amplitude modulation of the resulting data streams.

Keywords: microring resonator, all-optical signal processing, optical logic gate, demultiplexer, optical multiplexing, adder/subtractor.

1. Introduction

The growing demands in contemporary communication system paradigms are motivating an unprecedented development in ultra-high-speed optical networks to satiate the rapidly emergent needs of the industry. The bandwidth of the electronic circuits ultimately limits the speed of operation of the system [1]. Recently, silicon photonics has achieved a great development in optical computing and information processing due to high bandwidth, high-speed and parallelism properties of light [2–4]. At present in packet routing, the optical signal entering the router is converted to an electronic signal and

demultiplexed into lower-rate streams that are electronically routed in the switch core and then remultiplexed to a high-speed electronic signal that is the output from the router on the specified optical wavelength. This optical-electronic-optical conversion leads to router congestion and reduced capacity in today's networks [5]. So to accommodate the modern broadband network, very high-speed signal processing technologies must be developed not only for transmission lines, but also for transmission nodes. Multiplexing and demultiplexing [6–9] are two essential features in almost all the information processing, signal communication and networking systems, where a lot of information is being handled without any mutual disturbances.

In response to this, a number of schemes have been proposed for realization of multiplexers (MUXs) and demultiplexers (DEMUXs) both theoretically [5, 10, 11] and experimentally [12–14] with several bit rates, channel spacings, modulation formats, and other system considerations such as polarization diversity [15], twisting of the nonlinear fiber [16, 17], and depolarization of the clock pulses [18]. All-optical MUXs/DEMUXs were also studied using a cross-phase modulation (XPM) effect [19], multilayer interference filters [20] and fiber Bragg grating filters [21, 22]. A microring resonator (MRR) is also used to design all-optical MUXs where circuit design is more complex [23].

The increasingly high-speed digital optical system and optical processor requires an all-optical adder/subtractor unit to perform optical microoperations. All-optical adder/subtractor units have many potential applications in optical computing and information processing. Various architectures and algorithms for logical and arithmetic operations have been proposed in the field of optical/optoelectronic computing and parallel signal processing in last few decades [24–28]. Among different topologies, the proposed adder/subtractor units using MRR represent the most promising solution due to their ultra-compact size, less complex circuitry.

In the present paper, we propose and describe all-optical MUX/DEMUX, which utilize two silicon waveguide based MRRs. Optical resonators on planar platforms have been used to reduce the footprint of all-optical devices through recycling light within them, which increases the effective nonlinearity of these structures.

The paper is organized as follows: operational principle of all-optical 2×2 switch using MRR is discussed in Section 2. In Section 3, the theory, design, simulation results and discussion of the proposed schemes for multiplexing and demultiplexing are explained. Designating of half-adder/subtractor and comparator circuit using DEMUX circuit is also discussed in Section 4, and Section 5 concludes the paper.

2. Microring resonator based optical switch

The basic configuration of the silicon MRR [29–32] consisting of two straight bus waveguides coupled to a microring in between is shown in Fig. 1.

A ring resonator acts as an optical reservoir to accumulate the power. When the optical path length of a round trip is the integer multiple of effective wavelength, con-

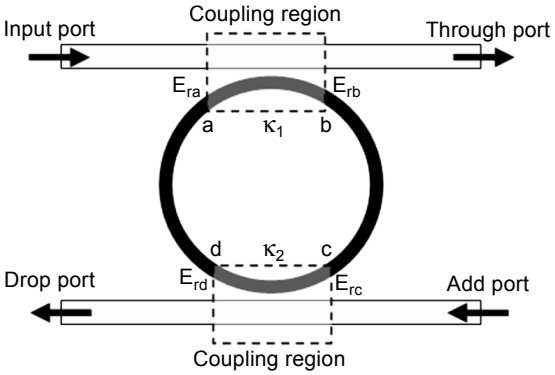

Fig. 1. Configuration of all-optical switch in MRR.

structive interference occurs and the MRR will have "ON" resonance. Initially, in the absence of pump pulse, the probe signal gets transmitted to a drop port. The resonance condition can be varied by applying pump power to the ring. The pump pulse induces the free carrier in the MRR due to two-photon absorption (TPA), which reduces the refractive index of the material through the plasma-dispersion effect and produces π-phase shift in one circle of the ring so that a probe light signal switches to through the port of MRR. After the passage of pump pulse, the resonance condition and probe signal relax back due to fast carrier recombination. The relaxation time is determined by the carrier lifetime of ~0.5 ns in the ring resonator [33]. Thus optical switching for a signal beam between two output ports (through port and drop port) can be realized.

First we can calculate the transfer function of the MRR shown in Fig. 1. We consider that the field coupling coefficient between the ring and the input bus is κ_1 and the field coupling coefficient between the output bus and the ring is κ_2. The wave propagation constant is κ_n, where $\kappa_n = 2\pi n_{\text{eff}}/\lambda$, and λ is the resonant wavelength of the ring, n_{eff} is the effective refractive index of the waveguide of the ring. The output electric fields at through and drop ports can be respectively written as [34, 35],

$$E_t = \frac{\sqrt{1-\kappa_1} - \sqrt{1-\kappa_2}\, x^2 \exp^2(j\varphi)}{1 - \sqrt{1-\kappa_1}\sqrt{1-\kappa_2}\, x^2 \exp^2(j\varphi)} E_{i_1} + \frac{-\sqrt{\kappa_1}\sqrt{\kappa_2}\, x \exp(j\varphi)}{1 - \sqrt{1-\kappa_1}\sqrt{1-\kappa_2}\, x^2 \exp^2(j\varphi)} E_{i_2} \tag{1}$$

$$E_d = \frac{-\sqrt{\kappa_1}\sqrt{\kappa_2}\, x \exp(j\varphi)}{1 - \sqrt{1-\kappa_1}\sqrt{1-\kappa_2}\, x^2 \exp^2(j\varphi)} E_{i_1} + \frac{\sqrt{1-\kappa_2} - \sqrt{1-\kappa_1}\, x^2 \exp^2(j\varphi)}{1 - \sqrt{1-\kappa_1}\sqrt{1-\kappa_2}\, x^2 \exp^2(j\varphi)} E_{i_2} \tag{2}$$

where $x = \exp(-\alpha L/2)$, $\varphi = \kappa_n L/2$, E_{i_1} and E_{i_2} are the input and add port field, respectively. The effective refractive index of Si-waveguide ring can be expressed as $n_{\text{eff}} = n_0 + n_2 I = n_0 + n_2 P/S$, where n_0 and n_2 are the linear and nonlinear refractive

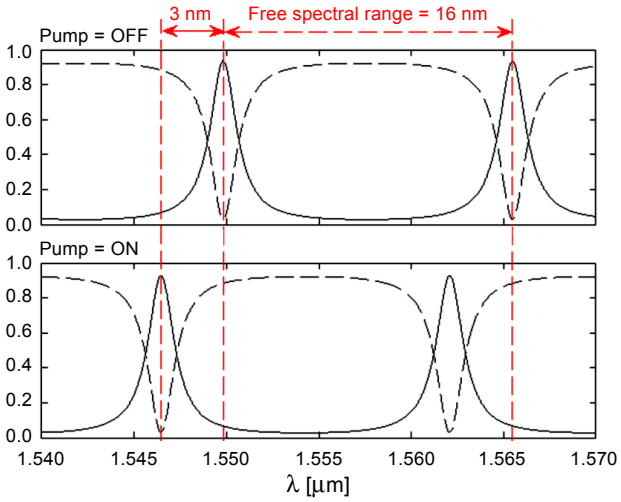

Fig. 2. Transfer function at through port (dashed line) and drop port (solid line) outputs.

indexes, respectively, I and P are the intensity and power of the optical pump signal, S is the effective cross-sectional area of the ring resonator. For simplification of the calculation of fields, the coupling losses are not taken into account.

We can calculate the transfer function at through port T_p and drop port T_d putting $E_{i_2} = 0$ as $T_p = |E_t|^2/|E_{i_1}|^2$ and $T_d = |E_d|^2/|E_{i_1}|^2$, respectively (see Fig. 2).

Now we calculate a phase shift and refractive index change due to the application of pump pulse. We consider the case under pumping of a ring by a pulsed laser, which induces TPA in the silicon material. This makes changes in the free carrier concentration including a change of electron concentration ΔN_e and a change of hole concentration ΔN_h.

The nonlinear refractive index change at the wavelength of 1.55 μm is given by [36, 37]

$$\Delta n = \Delta n_e + \Delta n_h = -\left[8.8 \times 10^{-22} \Delta N + 8.5 \times 10^{-22} (\Delta N)^{0.8}\right] \tag{3}$$

where $\Delta N = \Delta N_e = \Delta N_h$.

The negative sign in Eq. (3) shows that effectively it is a net decrease in the refractive index of the microring waveguide which causes a temporarily blue shift of the microring resonance wavelength.

The free-carrier concentration N in the silicon waveguide is generated by TPA, so its rate of generation is given by [38]

$$\frac{\mathrm{d}N}{\mathrm{d}t} = \frac{\beta I^2}{2h\nu} \tag{4}$$

where I is the light intensity, β is the TPA coefficient, and $h\nu$ is the photon energy.

Let us consider a Gaussian pump pulse of intensity $I = P\exp(-t^2/\tau^2)/S$ fall on the ring, where P is the peak power and τ is the pulse width at half-peak power. This pump power induces two-photon absorption in the materials of the silicon waveguide ring.

For Gaussian pulses, the relationship between the peak power P and the average power P_{avg} with pulse separation t_p and pulse width τ is [38]

$$\frac{P}{P_{\text{avg}}} = \frac{\sqrt{2}\, t_p}{\sqrt{\pi}\, \tau} \tag{5}$$

Then the free-carrier-concentration change created by a single pulse is given by

$$\Delta N = \frac{\beta}{2h\nu}\int_{-\infty}^{\infty}\left(\frac{P}{S}\right)^2 \exp\left(\frac{-4t^2}{\tau^2}\right)\mathrm{d}t = \frac{\beta\sqrt{\pi}\,\tau P^2}{4h\nu S^2} \tag{6}$$

Using Eqs. (3) and (6), the relationship between the refractive index and the average power of the pump light is obtained

$$\Delta n = -\left[8.8\times 10^{-22}\frac{\beta t_p^2}{2h\nu\sqrt{\pi}\,\tau S^2}P_{\text{avg}}^2 + 8.5\times 10^{-22}\left(\frac{\beta t_p^2}{2h\nu\sqrt{\pi}\,\tau S^2}P_{\text{avg}}^2\right)^{0.8}\right] \tag{7}$$

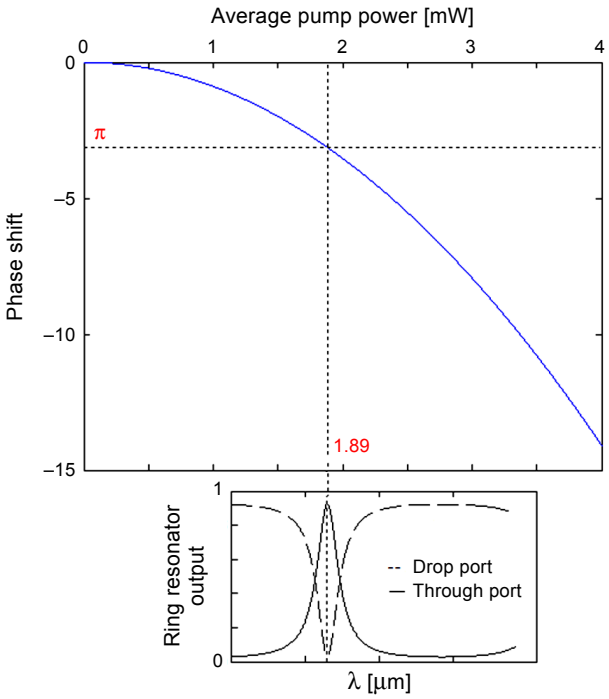

Fig. 3. Phase shift in the ring resonator as a function of average pump power.

The refractive index change results in a phase shift change of the signal light at 1.55 μm in one circle of the ring and is given by

$$\varphi = \frac{2\pi}{\lambda}\Delta nL \tag{8}$$

where L is the length of the ring.

The curve of a phase shift can be obtained from Eq. (8) using the following data: $\beta = 7.9 \times 10^{-10}$ cm/W, pump beam wavelength, $\lambda_p = 400$ nm, $\tau = 100$ fs, $t_p = 12.5$ ns, $h\nu = 49.725 \times 10^{-20}$ J, $L = 2\pi r = 44.5$ μm, $S = 450 \times 250$ nm^2, $n_2 = 4 \times 10^{-18}$ m^2/W. The graph for a phase shift with average pump power is shown in Fig. 3. It can be shown from Fig. 3 that when the phase shift approaches π, the average pump power required for switching is only 1.89 mW. We found from Fig. 2 the on-off ratio 14.95 dB and free spectral range of 16 nm.

3. Design of microring resonator based optical multiplexer/demultiplexer circuits

3.1. Architecture and principle of all-optical multiplexer

Multiplexer (MUX) transmits large number of information channels to a single common channel. A digital MUX is a combinational circuit that selects binary information from one of the many input channels by proper combination of a selection line and transmits to the output line. Because of that the digital MUXs are also called data selectors. Our proposed model is the optical implementation of the digital MUX. Different kind of complex logical expression can be easily implemented using MUX/DEMUX rather than discrete components. This kind of MUXs can also be used in communications like telephone network. In this regards, the block diagram for 4:1 MUX is shown in Fig. 4.

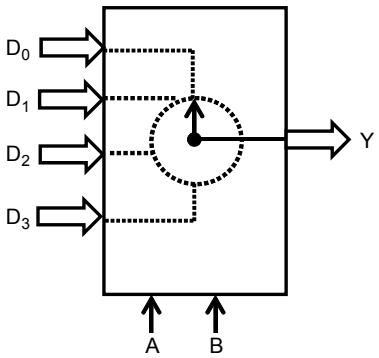

Fig. 4. Block diagram of a 4:1 MUX; D_0, D_1, D_2, D_3 – input data signal, A, B – control/selection line, Y – output.

The Boolean expression for the output of 4:1 MUX is given by

$$Y = \overline{A}\,\overline{B}D_0 + \overline{A}BD_1 + A\overline{B}D_2 + ABD_3 \tag{9}$$

The proposed architecture and the experimental setup of 4:1 MUX consisting of two MRRs only are shown in Figs. 5 and 6, respectively. Two MRRs are modulated by two independent optical pulse sequences A and B, respectively. The low and high level of optical pulse sequences applied to the MRRs defines logical 0 and 1, respectively. In or-

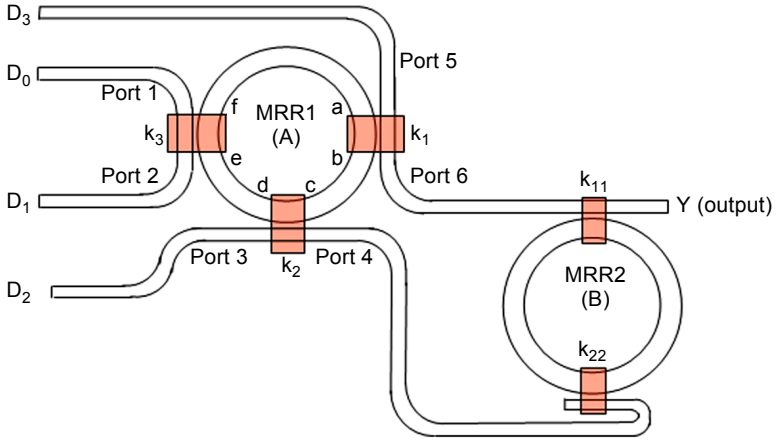

Fig. 5. All-optical 4:1 multiplexing scheme using ring resonator.

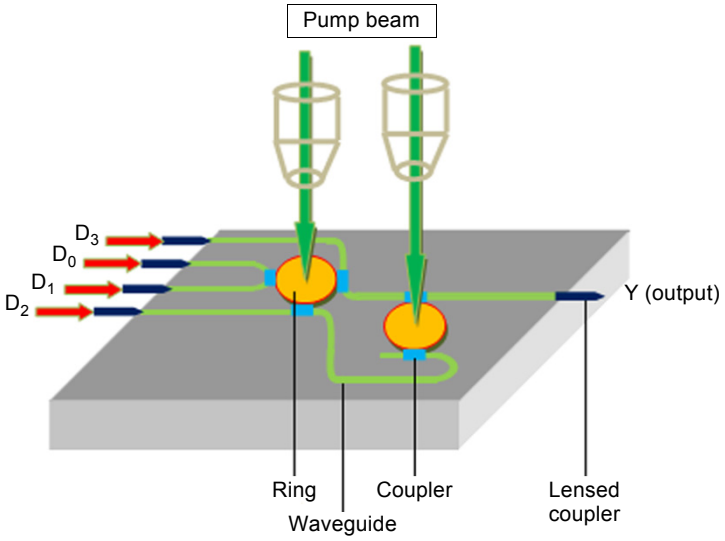

Fig. 6. Proposed experimental setup of 4:1 MUX using two MRRs.

der to establish the operational principle of the proposed MUX, firstly we introduce the principles of its two fundamental elements: MRR1 and MRR2. MRR2 behaves as 2×2 optical switch [39, 40]. When a low-level optical pump signal is applied to MRR2, it is on-resonance at λ and the optical signal coupled into its input port is directed to its drop port. When a high-level optical pump signal is applied to MRR2, it is off-resonance at λ and the optical signal coupled into its input port is directed to its through the port.

The same definition is also effective to the MRR1. It has six ports and three coupling regions. In principle, any port can be considered as the input port of the optical signal. In the proposed device, ports 1, 2, 3 and 5 behave as the input ports of the optical signal, and one of these four ports also behaves as the output port when the other port acts as the input port. When a low-level optical pump signal is applied to MRR1, it is on-resonance at λ. The half of the light signal coupled into port 1 is directed to port 4 and the remaining light signal directed to port 5. Similarly, light signals coupled to ports 2, 3 and 5 are directed to ports 6 and 3, ports 5 and 2, ports 3 and 1, respectively, when a low-level optical pump signal is applied. When a high-level optical pump signal is applied to MRR1, it is off-resonance at λ. The optical signals coupled into ports 1, 2, 3 and 5 are directed to ports 2, 1, 4 and 6, respectively.

According to the above definitions, the principle of the proposed device can be summarized as follows.

When the optical control pulses applied to MRR1 and MRR2 are at a low level ($A = 0$, $B = 0$), both MRR1 and MRR2 are on-resonance. The input signal D_0 at port 1 and D_1 at port 2 of MRR1 are firstly directed to ports 4 and 6, respectively. Ports 4 and 6 of MRR1 act as an add port and input port of MRR2, respectively. As the control pulse at MRR2 is also at a low level, port 4 signal is directed to the output port Y which is equivalent to D_0 input.

When the optical control pulses applied to MRR1 and MRR2 are respectively at a low and high level ($A = 0$, $B = 1$), MRR1 is on-resonance and MRR2 is off-resonance. The input signal D_0 at port 1 and D_1 at port 2 of MRR1 are firstly directed to ports 4 and 6, respectively. As a control pulse at MRR2 is at a high-level, port 6 signal is directed to the output port Y which is equivalent to D_1 input.

When the optical control pulses applied to MRR1 and MRR2 are respectively at a high and low level ($A = 1$, $B = 0$), MRR1 is off-resonance and MRR2 is on-resonance. The input signals D_2 at port 3 and D_3 at port 5 of MRR1 are firstly directed to ports 4 and 6, respectively. As the control pulse at MRR2 is at a low-level, port 4 signal is directed to the output port Y which is equivalent to D_2 input.

When the optical control pulses applied to MRR1 and MRR2 are at a high-level ($A = 1$, $B = 1$), both MRR1 and MRR2 are off-resonance. The input signal D_2 at port 3 and D_3 at port 5 of MRR1 are firstly directed to ports 4 and 6, respectively. As the control pulse at MRR2 is also at a high-level, port 6 signal is directed to the output port Y which is equivalent to D_3 input. So the proposed model can perform the 4:1 multiplexing using 2 control pulses.

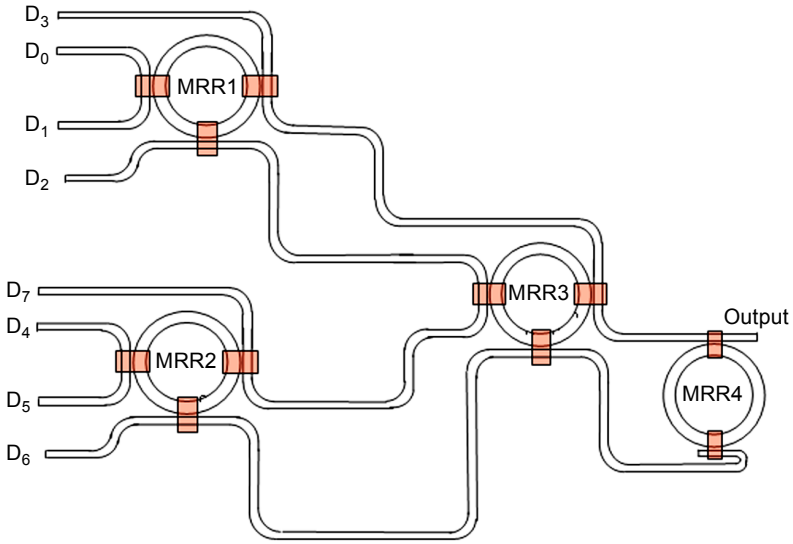

Fig. 7. All-optical 8:1 multiplexing scheme using a ring resonator.

The order of MUXs can easily be increased by placing MRRs in front of MRR1 of Fig. 5. For designing 8:1 MUX, two (4 input, 2 output) MRRs should be placed in front of MRR1 of Fig. 5 and the outputs should be connected to the inputs of MRR1. The configuration of 8:1 MUX is shown in Fig. 7.

3.2. Mathematical model for 4:1 multiplexer

When D_0 input is only present at MRR1 as shown in Fig. 5, the electric field at point e can be written as

$$E_e = j\sqrt{k_3}\, D_0 + E_a e^{2x}\sqrt{1-k_3} \tag{10}$$

where E_a is the electric field at point a and given by

$$E_a = E_c e^{x}\sqrt{1-k_1} \tag{11}$$

The electric field at point c can be written as

$$E_c = E_e e^{x}\sqrt{1-k_2} \tag{12}$$

therefore,

$$E_e = \frac{j\sqrt{k_3}\, D_0}{1-\sqrt{(1-k_1)(1-k_2)(1-k_3)}\, e^{4x}} \tag{13}$$

The electric field at port 4 is given by

$$E_{d_0} = j\sqrt{k_2}\,E_e e^{x} \tag{14}$$

where k_1, k_2 and k_3 are the coupling coefficients of MRR1 and $x = -(\alpha/2)(L/4) - jk_nL/4$ as shown in Fig. 5, $k_n = 2\pi n_{\text{eff}_1}/\lambda$, the effective refractive index of Si-waveguide ring MRR1 can be expressed as $n_{\text{eff}_1} = n_0 + n_2 I_1 = n_0 + n_2 P_1/S$, where n_0 and n_2 are the linear and nonlinear refractive indexes, respectively, I_1 and P_1 are the intensity and power of the optical pump signal used for MRR1.

Similarly when D_1 input is present only, the electric field at port 6 is given by

$$E_{t_1} = j\sqrt{k_1}\,E_f e^{2x} \tag{15}$$

where the electric field at point f can be written as

$$E_f = \frac{j\sqrt{k_3}\,D_1}{1 - \sqrt{(1-k_1)(1-k_2)(1-k_3)}\,e^{4x}} \tag{16}$$

When D_2 input is present only, the electric field at port 4 is given by

$$E_{d_2} = D_2\sqrt{1-k_2} + j\sqrt{k_2}\,e^{x}E_{e_1} \tag{17}$$

where the electric field at point e can be written as

$$E_{e_1} = \frac{j\sqrt{k_2(1-k_1)(1-k_3)}\,e^{3x}}{1 - \sqrt{(1-k_1)(1-k_2)(1-k_3)}\,e^{4x}} \tag{18}$$

Similarly when D_3 input is present only, the electric field at port 6 is given by

$$E_{t_3} = D_3\sqrt{1-k_1} + j\sqrt{k_1}\,e^{2x}E_{g_1} \tag{19}$$

where the electric field at point g can be written as

$$E_{g_1} = \frac{j\sqrt{k_1(1-k_2)(1-k_3)}\,e^{2x}}{1 - \sqrt{(1-k_1)(1-k_2)(1-k_3)}\,e^{4x}} \tag{20}$$

When all the four inputs are present, the electric field at port 4 can be written as

$$E_d = E_{d_0} + E_{d_2} \tag{21}$$

When all the four inputs are present, the electric field at port 6 is given by

$$E_t = E_{t_1} + E_{t_3} \tag{22}$$

The field at the through port of MRR2 can be written as

$$E_y = \frac{\sqrt{1-k_{11}} - \sqrt{1-k_{22}}\, e^{4x_1}}{1 - \sqrt{1-k_{11}}\,\sqrt{1-k_{22}}\, e^{4x_1}} E_t - \frac{\sqrt{k_{11}}\,\sqrt{k_{22}}\, e^{2x_1}}{1 - \sqrt{1-k_{11}}\,\sqrt{1-k_{22}}\, e^{4x_1}} E_d \tag{23}$$

where k_{11} and k_{22} are the coupling coefficient of MRR2, E_d and E_t are the ports 4 and 6 outputs of MRR1, respectively, and $x_1 = -(\alpha/2)(L/4) - jk_{n_1}L/4$, $k_{n_1} = 2\pi n_{\text{eff}_2}/\lambda$, the effective refractive index of Si-waveguide ring MRR2 can be expressed as $n_{\text{eff}_2} = n_0 + n_2 I_2 = n_0 + n_2 P_2/S$, where n_0 and n_2 are the linear and nonlinear refractive indexes, respectively, I_2 and P_2 are the intensity and power of the optical pump signal used for MRR2.

The above equations are used to design an all-optical data multiplexing scheme using MRRs.

3.3. Architecture and principle of all-optical demultiplexer

Proposed architecture and experimental setup of 1:4 DEMUX consisting of two MRRs only are shown in Figs. 8 and 9, respectively. Two MRRs are modulated by two independent optical pulse sequences *A* and *B*, respectively. A monochromatic wave with working wavelength λ is modulated by two optical pump pulse trains *A* and *B* applied to the two MRRs, respectively. The optical pulse trains appearing at different output ports depend on different combinations of the optical pump pulses applied to MRR1 and MRR2.

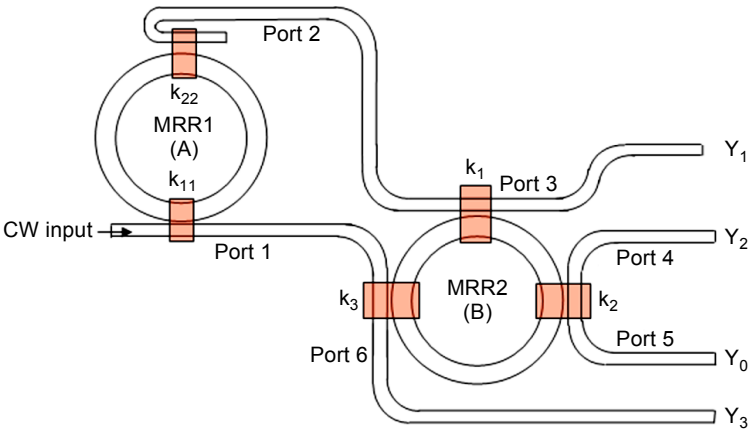

Fig. 8. All-optical 1:4 demultiplexing scheme using a ring resonator.

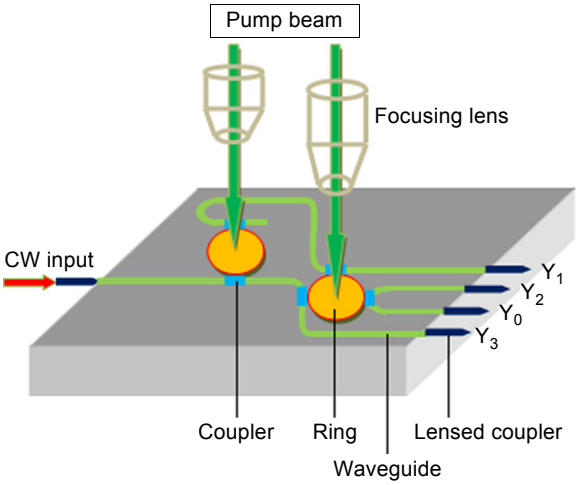

Fig. 9. Proposed experimental setup of 1:4 DEMUX using a two MRRs.

According to the definition of MRR as discussed in Section 2, when both pump pulses are at a low level ($A = 0$ and $B = 0$), both rings are off resonance and the logical high level (1) is achieved at the output port Y_0 and the logical low level (0) is achieved at three other output ports Y_1, Y_2, Y_3. Logical 1 is achieved at the output port Y_1 and logical 0s are achieved at three other output ports Y_0, Y_2, and Y_3 when $A = 0$, $B = 1$. Logical 1 is achieved at the output port Y_2 and logical 0s are achieved at three other output ports Y_0, Y_1, and Y_3 when $A = 1$, $B = 0$. When $A = 1$ and $B = 1$, logical 1 is achieved at the output port Y_3 and logical 0s are achieved at three other output ports Y_0, Y_1, and Y_2. So, the proposed device can choose the demultiplexed channel based on different combinations of pump pulses.

The order of DEMUX can easily be increased by placing MRRs in a reverse order to that of MUX.

3.4. Mathematical model for demultiplexer

The field at the through port and drop port of MRR1 can be written as [28]

$$E_{t_0} = \frac{\sqrt{1-k_{11}} - \sqrt{1-k_{22}}\, e^{4x_1}}{1 - \sqrt{1-k_{11}}\,\sqrt{1-k_{22}}\, e^{4x_1}} E_{i_1} - \frac{\sqrt{k_{11}}\,\sqrt{k_{22}}\, e^{2x_1}}{1 - \sqrt{1-k_{11}}\,\sqrt{1-k_{22}}\, e^{4x_1}} E_{i_2} \tag{24}$$

$$E_{d_0} = -\frac{\sqrt{k_{11}}\,\sqrt{k_{22}}\, e^{2x_1}}{1 - \sqrt{1-k_{11}}\,\sqrt{1-k_{22}}\, e^{4x_1}} E_{i_1} + \frac{\sqrt{1-k_{11}} - \sqrt{1-k_{22}}\, e^{4x_1}}{1 - \sqrt{1-k_{11}}\,\sqrt{1-k_{22}}\, e^{4x_1}} E_{i_2} \tag{25}$$

where E_{i_1} is CW input at the input port of MRR1 and the add port field, E_{i_2} is considered as zero.

The field at ports 3, 4, 5, and 6 of MRR2 can be calculated in a similar way as discussed in Section 3.2.

The field at port 3 (output channel Y_1) can be written as

$$E_{t_1} = \frac{-k_1\sqrt{(1-k_2)(1-k_3)}\, e^{4x}}{1-\sqrt{(1-k_1)(1-k_2)(1-k_3)}\, e^{4x}} E_{t_0} + \sqrt{1-k_1}\, E_{t_0} \tag{26}$$

The field at port 4 (output channel Y_2) can be written as

$$E_{t_2} = \frac{-\sqrt{k_2 k_3}\, e^{2x}}{1-\sqrt{(1-k_1)(1-k_2)(1-k_3)}\, e^{4x}} E_{d_0} \tag{27}$$

The field at port 5 (output channel Y_0) can be written as

$$E_{t_3} = \frac{-\sqrt{k_1 k_2}\, e^{x}}{1-\sqrt{(1-k_1)(1-k_2)(1-k_3)}\, e^{4x}} E_{t_0} \tag{28}$$

The field at port 6 (output channel Y_3) can be written as

$$E_{t_4} = \frac{-k_3\sqrt{(1-k_1)(1-k_2)}\, e^{4x}}{1-\sqrt{(1-k_1)(1-k_2)(1-k_3)}\, e^{4x}} E_{d_0} + \sqrt{1-k_3}\, E_{d_0} \tag{29}$$

The above equations are used to design an all-optical data demultiplexing scheme using MRRs.

3.5. Simulation results for multiplexer and demultiplexer

A silicon waveguide based MRR is a powerful device to realize the ultrafast all-optical switch. The advantage of silicon waveguide based MRR is that the overall losses can be relatively low [41]. Pure silicon has an absorption loss much smaller than 0.1 dB/cm at the wavelength of 1.55 μm. Scattering loss is also very low. Curvature loss is in negligible levels. Insertion loss is also very low at the wavelength of 1.55 μm. A choice of coupling coefficients of MRR1 $k_1 = k_2 = k_3 = 0.33$ and coupling coefficients of MRR2 $k_{11} = k_{22} = 0.22$ is considered in the present study and the other optimized parameters as discussed in Section 2. The practical realization is very difficult because the coupling coefficient cannot be determined with the high accuracy. One possible solution would be to use tunable couplers. We choose probe input beam power 0.1 mW such that there is no variation of refractive index of the material of MRR for the input probe beam. The simulated result of all-optical 4:1 MUXs (using MATLAB) is reported in Fig. 10. Result is also given in tabular form as shown in Table 1. The threshold value at the output for the multiplexing scheme is considered as 0.01 mW. Simulation result

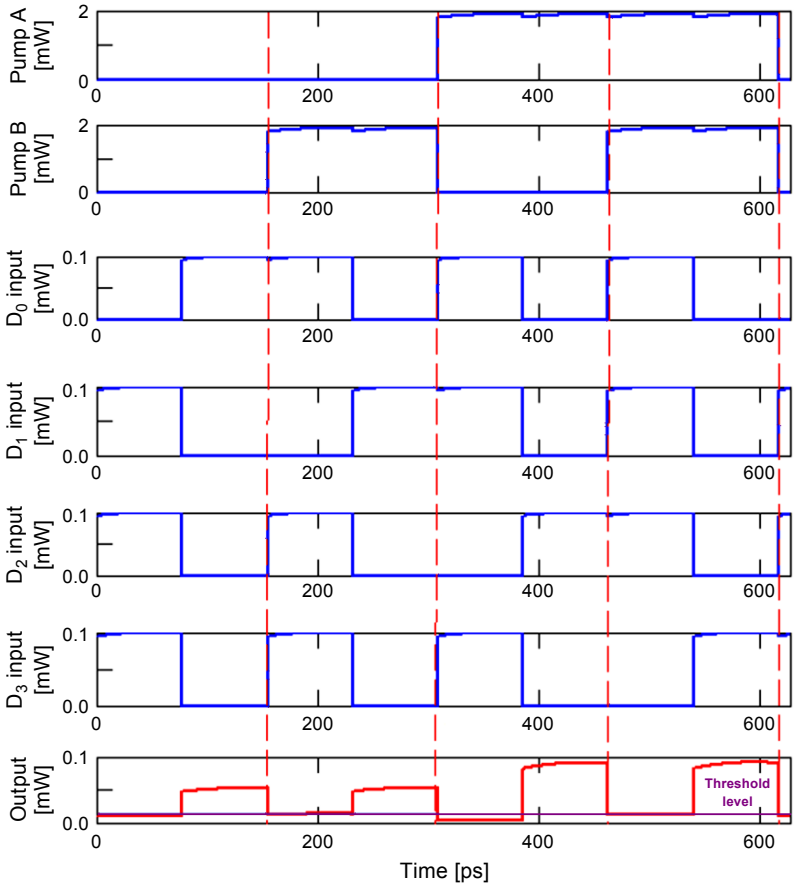

Fig. 10. Simulation output of 4:1 MUX.

T a b l e 1. Logical truth table of the proposed MUX and theoretical optical power levels at the input and output (X = do not care).

Select (control) inputs		Data inputs				
A	*B*	D_0	D_1	D_2	D_3	Output *Y*
0 (0 mW)	0 (0 mW)	0 (0 mW)	X	X	X	0 (0.01 mW)
0 (0 mW)	0 (0 mW)	1 (0.1 mW)	X	X	X	0 (0.052 mW)
0 (0 mW)	1 (1.89 mW)	X	0 (0 mW)	X	X	0 (0.011 mW)
0 (0 mW)	1 (1.89 mW)	X	1 (0.1 mW)	X	X	1 (0.052 mW)
1 (1.89 mW)	0 (0 mW)	X	X	0 (0 mW)	X	0 (0.004 mW)
1 (1.89 mW)	0 (0 mW)	X	X	1 (0.1 mW)	X	1 (0.092 mW)
1 (1.89 mW)	1 (1.89 mW)	X	X	X	0 (0 mW)	0 (0.01 mW)
1 (1.89 mW)	1 (1.89 mW)	X	X	X	1 (0.1 mW)	1 (0.092 mW)

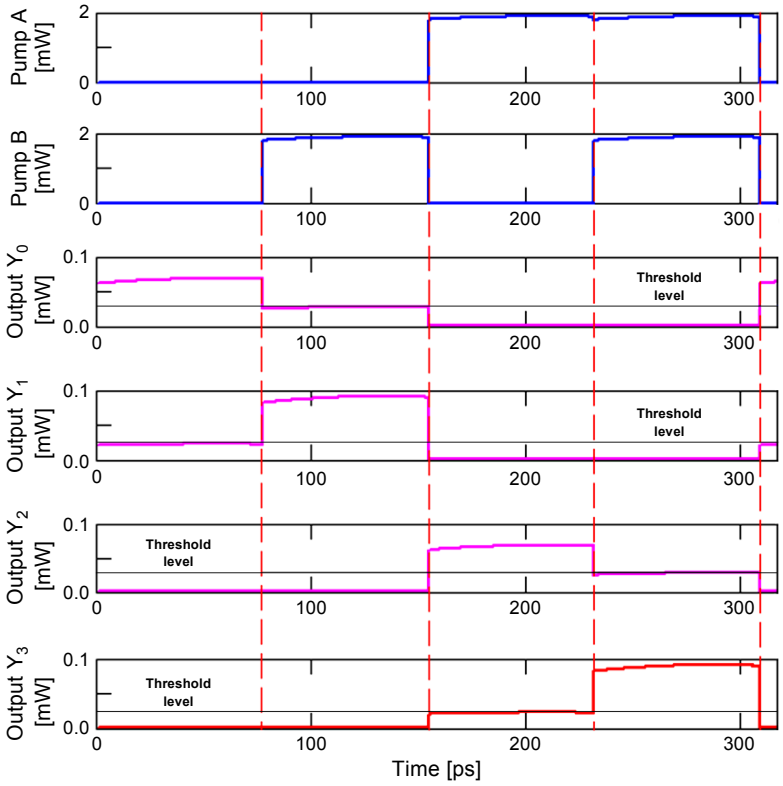

Fig. 11. Simulation output of 1:4 DEMUX.

of the optical DEMUX scheme is shown in Fig. 11. Result is also given in tabular form as shown in Table 2. The threshold value at the output for the demultiplexing scheme is considered as 0.02 mW. Data rate of the circuit for simulation is considered as 100 Gbps and maximum speed can be extended up to 250 Gbps [42, 43]. The carrier lifetime in microcavities drastically decreases due to surface recombination and thus limits the speed of the carrier-based switching [44].

T a b l e 2. Logical truth table of the proposed DEMUX and theoretical optical power levels at the input and output.

Select (control) inputs		Data inputs	Output Y_0	Output Y_1	Output Y_2	Output Y_3
A	*B*					
0 (0 mW)	0 (0 mW)	1 (0.1 mW)	1 (0.07 mW)	0 (0.02 mW)	0 (0 mW)	0 (0 mW)
0 (0 mW)	1 (1.89 mW)	1 (0.1 mW)	0 (0.02 mW)	1 (0.091 mW)	0 (0 mW)	0 (0 mW)
1 (1.89 mW)	0 (0 mW)	1 (0.1 mW)	0 (0 mW)	0 (0 mW)	1 (0.069 mW)	0 (0.02 mW)
1 (1.89 mW)	1 (1.89 mW)	1 (0.1 mW)	0 (0 mW)	0 (0 mW)	0 (0.02 mW)	1 (0.91 mW)

4. Design of microring resonator based optical half-adder/subtractor and comparator circuits

Figures 8 and 9 for DEMUX circuit can also be used for designing all-optical half -adder/subtractor and comparator [45–48]. In the half-adder, two outputs are represented by Sum = $\overline{X}\,Y + X\,\overline{Y}$ and Carry = XY. The half-subtractor has also two outputs

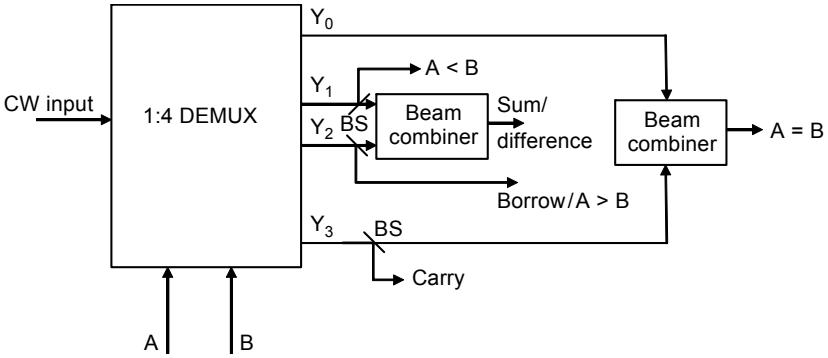

Fig. 12. Block diagram of the half-adder/subtractor and comparator circuit using 1:4 DEMUX; BS – beam splitter.

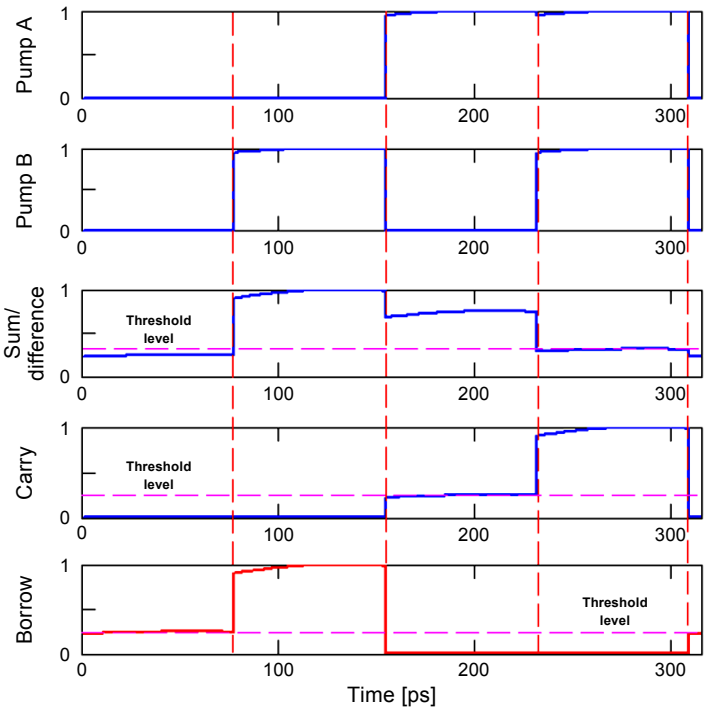

Fig. 13. Normalized simulation output of the half-adder/subtractor circuit.

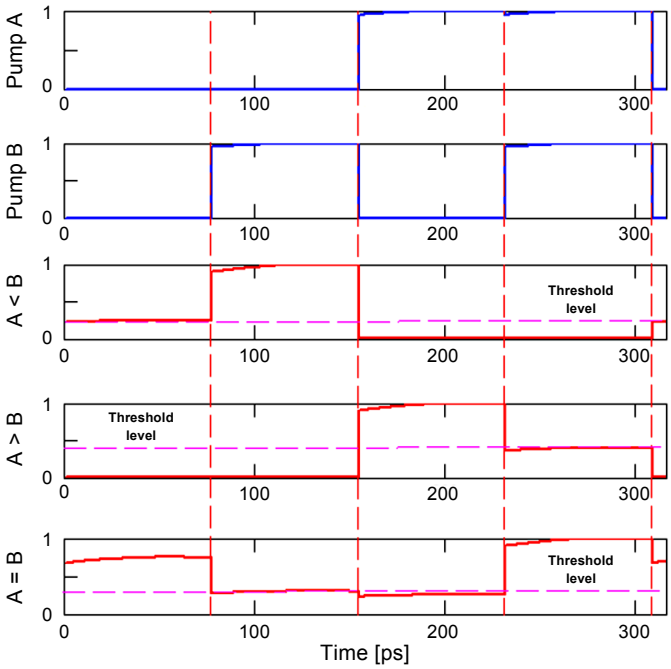

Fig. 14. Normalized simulation output of comparator circuit.

and is represented by Difference = $\overline{X}\,Y + X\,\overline{Y}$ and Borrow = $X\,\overline{Y}$. So the XOR output simultaneously gives the result of sum and difference. The XOR operation can be performed by combining Y_1 and Y_2 outputs. At the same time Y_3 and Y_2 give the carry bit and borrow bit respectively. Comparison between two binary data is often required in many data processing systems to control/drive the physical variable towards the reference value. Using the same cascaded MRR (Figs. 8 and 9) we can compare the two single bit binary numbers and generate one of the following outputs: $A = B$, $A > B$ and $A < B$. The output $A > B$ can be obtained from Y_2 terminal, $A < B$ can be obtained from Y_1 terminal and $A = B$ can be obtained by combining Y_0 and Y_3 outputs. The block diagram of half-adder/subtractor and comparator is shown in Fig. 12. Simulation results for half-adder/subtractor and comparator are shown in Figs. 13 and 14, respectively. Logical truth tables of the proposed circuits are given in Table 3.

T a b l e 3. Logical truth table of the half-adder/subtractor and comparator circuits.

Select (control) inputs		Outputs					
A	B	Sum/difference	Carry	Borrow	$A > B$	$A < B$	$A = B$
0	0	0	0	0	0	0	1
0	1	1	0	1	0	1	0
1	0	1	0	0	1	0	0
1	1	0	1	0	0	0	1

5. Discussion

High extinction ratio (ER) makes the ultrafast all-optical logic circuit suitable to be exploited to control all-optical switch. The high value of ER distinguishes the high (1) level to the low (0) level very clearly. The extinction ratio is defined as [49–51],

$$\text{ER (dB)} = 10 \log\left(\frac{P^1_{\text{min}}}{P^0_{\text{max}}}\right) \tag{30}$$

where P^1_{min} and P^0_{max} are the minimum and maximum values of the peak intensity of high (1) and low (0) level, respectively. We have plotted the extinction ratio *vs.* the different coupling coefficient with constant radius for both MUX and DEMUX circuits and is shown in Fig. 15**a**. Similarly we have also plotted ER *vs.* radius with constant coupling coefficient for both circuits, which is shown in Fig. 15**b**. The maximum value of ER is obtained as 7.16 dB at the optimum operating point.

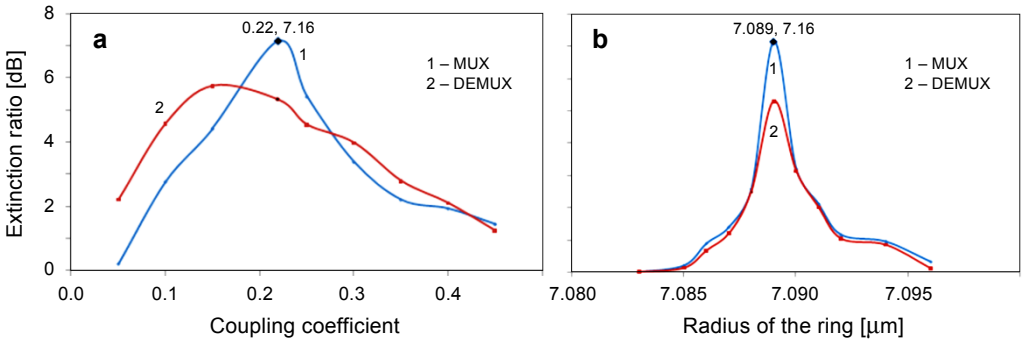

Fig. 15. Extinction ratio *vs.* coupling coefficient (**a**) and radius of the ring (**b**).

The output contrast ratio (CR) is defined as the ratio of the mean value of output intensity for 1 (P^1_{mean}) to the mean output intensity for 0 (P^0_{mean}), and is given as (in decibel) [49–51]

$$\text{CR (dB)} = 10 \log\left(\frac{P^1_{\text{mean}}}{P^0_{\text{mean}}}\right) \tag{31}$$

For the optimum performance, the CR must be as high as possible so that the main fraction of input can exist at the output. We have plotted the CR *vs.* the different coupling coefficient with constant radius for both MUX and DEMUX circuits and is shown in Fig. 16**a**. Similarly we have also plotted CR *vs.* radius with constant coupling coefficient for both circuits which is shown in Fig. 16**b**. The maximum value of CR is obtained as 10.71 dB in this case at the optimum operating point.

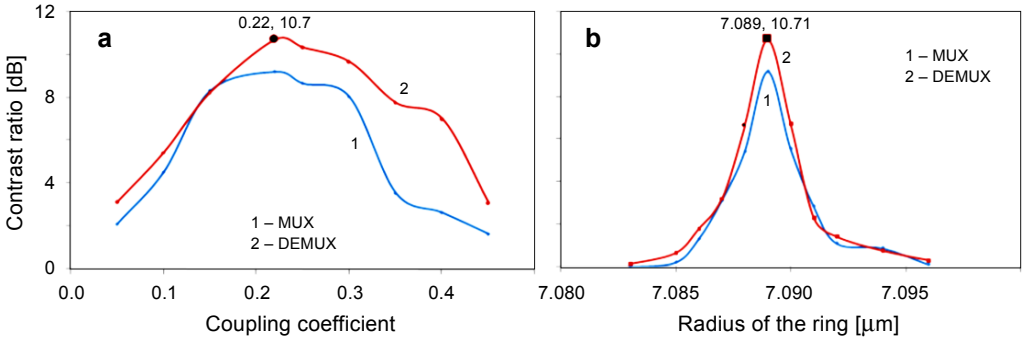

Fig. 16. Contrast ratio *vs.* coupling coefficient (**a**) and radius of the ring (**b**).

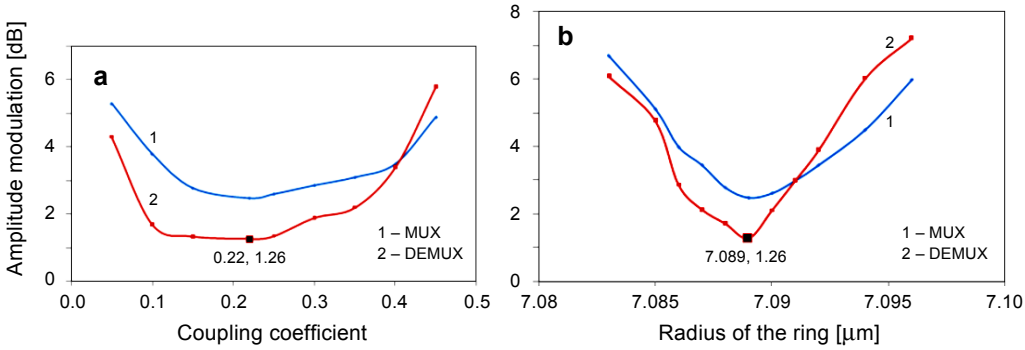

Fig. 17. Amplitude modulation *vs.* coupling coefficient (**a**) and radius of the ring (**b**).

The amplitude modulation (AM) can be defined as [49–51],

$$\text{AM (dB)} = 10 \log\left(\frac{P^1_{\max}}{P^1_{\min}}\right) \tag{32}$$

where $P^1_{\max}$ and $P^1_{\min}$ are the maximum and minimum value of intensity at high (1) level. In Fig. 17**a** we have plotted AM *vs.* coupling coefficient with constant radius for two logic circuits. Similarly in Fig. 17**b** we have plotted AM *vs.* radius with constant coupling coefficient for both circuits. The minimum value of AM is obtained as 1.26 dB at the optimum operating point, though the minimum for the AM should be lower than 1 dB [52] for better performance. The AM can be improved by means of additional passive MRR detuning [53].

6. Conclusion

We have proposed ultrafast optical MUX and DEMUX networks based on two MRRs as a feasible means of achieving a highly capable next-generation all-optical packet

-switched network which provides simple network management and self-routing of packets. The same DEMUX circuit is used to design the half-adder/subtractor and single bit comparator. The proposed schemes can easily and successfully be extended and implemented for higher order by proper incorporation of ring resonator based optical switches. Numerical simulation results confirming the described methods are also given in this paper. The theoretical model developed and the numerical results obtained may help in designing all-optical signal processing techniques and they are expected to play important roles in constructing future all-optical photonic networks in the 21st century. The variation of contrast ratio (CR), extinction ratio (ER) and amplitude modulation (AM) have been investigated and the noted values of CR, ER and AM are 10.71, 7.16 and 1.26 dB, respectively, at the optimum operating point.

References

[1] CAULFIELD H.J., DOLEV S., *Why future supercomputing requires optics*, Nature Photonics **4**(5), 2010, pp. 261–263.

[2] YONGHUI TIAN, LIN YANG, LEI ZHANG, RUIQIANG JI, JIANFENG DING, PING ZHOU, WEIWEI ZHU, YANGYANG LU, *Directed optical half-adder based on two cascaded microring resonators*, IEEE Photonics Technology Letters **24**(8), 2012, pp. 643–645.

[3] WEN Y.H., KUZUCU O., TAIGE HOU, LIPSON M., GAETA A.L., *All-optical switching of a single resonance in silicon ring resonators*, Optics Letters **36**(8), 2011, pp. 1413–1415.

[4] KUMAR S., BISHT A., SINGH G., CHOUDHARY K., RAINA K.K., AMPHAWAN A., *Design of 1-bit and 2-bit magnitude comparators using electro-optic effect in Mach–Zehnder interferometers*, Optics Communications **357**, 2015, pp. 127–147.

[5] HIRAYAMA T., MIYAZAWA T., FURUKAWA H., HARAI H., *Optical and electronic combined buffer architecture for optical packet switches*, Journal of Optical Communications and Networking **7**(8), 2015, pp. 776–784.

[6] YANQIAO XIE, SHIMING GAO, SAILING HE, *Simultaneous all-optical, error-free time-division demultiplexing and NRZ-to-RZ format conversion using a silicon-on-insulator waveguide*, [In] *2012 17th Opto-Electronics and Communications Conference (OECC)*, IEEE Conference Publications, 2012, pp. 241–242.

[7] IBRAHIM T.A., VAN V., HO P.-T., *All-optical time-division demultiplexing and spatial pulse routing with a GaAs/AlGaAs microring resonator*, Optics Letters **27**(10), 2002, pp. 803–805.

[8] ZHAN-QIANG HUI, JIAN-GUO ZHANG, *Wavelength conversion, time demultiplexing and multicasting based on cross-phase modulation and four-wave mixing in dispersion-flattened highly nonlinear photonic crystal fiber*, Journal of Optics **14**(5), 2012, article 055402.

[9] ZHAN-QIANG HUI, JIAN-GUO ZHANG, JIA-MIN GONG, MENG LIANG, MEI-ZHI ZHANG, YI YANG, FENG-TAO HE, JI-HONG LIU, *Demonstration of 40 Gbit/s all-optical return-to-zero to nonreturn-to -zero format conversion with wavelength conversion and dual-channel multicasting based on multiple cross-phase modulation in a highly nonlinear fiber*, Optical Engineering **52**(5), 2013, article 055002.

[10] KUINDERSMA P.I., LEIJTENS X.J.M., VAN ZANTVOORT J.H.C., DE WAARDT H., *A dual purpose, all optical multiplexer circuit in InP, for multiplexing clock and NRZ data, and for transmultiplexing WDM to TDM*, Optics Express **20**(28), 2012, pp. 29577–29589.

[11] SETHI P., ROY S., *All-optical ultrafast switching in 2×2 silicon microring resonators and its application to reconfigurable DEMUX/MUX and reversible logic gates*, Journal of Lightwave Technology **32**(12), 2014, pp. 2173–2180.

[12] KOONEN A.M.J., HAOSHUO CHEN, VAN DEN BOOM H.P.A., RAZ O., *Silicon photonic integrated mode multiplexer and demultiplexer*, IEEE Photonics Technology Letters **24**(21), 2012, pp. 1961–1964.

[13] FABBRI S.J., SYGLETOS S., PERENTOS A., PINCEMIN E., SUGDEN K., ELLIS A.D., *Experimental implementation of an all-optical interferometric drop, add, and extract multiplexer for superchannels*, Journal of Lightwave Technology **33**(7), 2015, pp. 1351–1357.

[14] LI J., LIU W., WANG Z., WEN F., LI L., LIU H., ZHENG H., ZHANG Y., *All-optical routing and space demultiplexer via four-wave mixing spatial splitting*, Applied Physics B **106**(2), 2012, pp. 365–371.

[15] CHEN C.P., DRISCOLL J.B., GROTE R.R., SOUHAN B., OSGOOD R.M., BERGMAN K., *Mode and polarization multiplexing in a Si photonic chip at 40 Gb/s aggregate data bandwidth*, IEEE Photonics Technology Letters **27**(1), 2015, pp. 22–25.

[16] LIANG Y., LOU J.W., ANDERSEN J.K., STOCKER J.C., BOYRAZ O., ISLAM M.N., NOLAN D.A., *Polarization-insensitive nonlinear optical loop mirror demultiplexer with twisted fiber*, Optics Letters **24**(11), 1999, pp. 726–728.

[17] IBARRA-ESCAMILLA B., KUZIN E.A., ZACA-MORAN P., MENDEZ-MARTINEZ F., HAUS J.W., POTTIEZ O., ROJAS-LAGUNA R., *Experimental investigation of the nonlinear optical loop mirror with low-birefringence, twisted fiber*, [In] *Conference on Lasers and Electro-Optics/Quantum Electronics and Laser Science and Photonic Applications Systems Technologies*, Optical Society of America, 2005, article JTuC7.

[18] FUJIWARA M., SUZUKI H., IWATSUKI K., *Narrow-bandwidth polarization-scrambling technique using delay-coupled binary phase pulse for carrier-distributed WDM networks*, Journal of Lightwave Technology **24**(7), 2006, pp. 2798–2805.

[19] UCHIYAMA K., KAWANISHI S., SARUWATARI M., *Multiple-channel output all-optical OTDM demultiplexer using XPM-induced chirp compensation (MOXIC)*, Electronics Letters **34**(6), 1998, pp. 575–576.

[20] OTANI T., ANTONIADES N., ROUDAS I., STERN T.E., *Cascadability of passband-flattened arrayed waveguide-grating filters in WDM optical networks*, IEEE Photonics Technology Letters **11**(11), 1999, pp. 1414–1416.

[21] BOCK H., LEISCHING P., RICHTER A., STOLL D., FISCHER G., *System impact of cascaded optical add/drop multiplexers based on tunable fiber Bragg gratings*, [In] *2000 Optical Fiber Communication Conference*, Vol. 2, IEEE Conference Publications, 2000, pp. 296–298.

[22] NYKOLAK G., EGGLETON B.J., LENZ G., STRASSER T.A., *Dispersion penalty measurements of narrow fiber Bragg gratings at 10 Gb/s*, IEEE Photonics Technology Letters **10**, 1998, pp. 1319–1321.

[23] RAKSHIT J.K., ROY J.N., *Design of all-optical time-division multiplexing scheme with the help of microring resonator*, Optica Applicata **44**(1), 2014, pp. 39–54.

[24] ROY J.N., *Mach–Zehnder interferometer-based tree architecture for all-optical logic and arithmetic operations*, Optik – International Journal for Light and Electron Optics **120**(7), 2009, pp. 318–324.

[25] GAYEN D.K., PAL R.K., ROY J.N., *All-optical adder/subtractor based on terahertz optical asymmetric demultiplexer*, Chinese Optics Letters **7**(6), 2009, pp. 530–533.

[26] KUMAR S., CHANDERKANTA, AMPHAWAN A., *Design of parity generator and checker circuit using electro-optic effect of Mach–Zehnder interferometers*, Optics Communications **364**, 2016, pp. 195–224.

[27] GAYEN D.K., BHATTACHRYYA A., CHATTOPADHYAY T., ROY J.N., *Ultrafast all-optical half adder using quantum-dot semiconductor optical amplifier-based Mach–Zehnder interferometer*, Journal of Lightwave Technology **30**(21), 2012, pp. 3387–3393.

[28] RAKSHIT J.K., CHATTOPADHYAY T., ROY J.N., *Design of ring resonator based all optical switch for logic and arithmetic operations – a theoretical study*, Optik – International Journal for Light and Electron Optics **124**(23), 2013, pp. 6048–6057.

[29] QIANFAN XU, SOREF R., *Reconfigurable optical directed-logic circuits using microresonator-based optical switches*, Optics Express **19**(6), 2011, pp. 5244–5259.

[30] LIN YANG, LEI ZHANG, CHUNMING GUO, JIANFENG DING, *XOR and XNOR operations at 12.5 Gb/s using cascaded carrier-depletion microring resonators*, Optics Express **22**(3), 2014, pp. 2996–3012.
[31] SHAOWU CHEN, LIBIN ZHANG, YONGHAO FEI, TONGTONG CAO, *Bistability and self-pulsation phenomena in silicon microring resonators based on nonlinear optical effects*, Optics Express **20**(7), 2012, pp. 7454–7468.
[32] QIAOSHAN CHEN, FANFAN ZHANG, LEI ZHANG, YONGHUI TIAN, PING ZHOU, JIANFENG DING, LIN YANG, *1 Gbps directed optical decoder based on two cascaded microring resonators*, Optics Letters **39**(14), 2014, pp. 4255–4258.
[33] QIANFAN XU, LIPSON M., *All-optical logic based on silicon micro-ring resonators*, Optics Express **15**(3), 2007, pp. 924–929.
[34] RAKSHIT J.K., ROY J.N., *Micro-ring resonator based all-optical reconfigurable logic operations*, Optics Communications **321**, 2014, pp. 38–46.
[35] RAKSHIT J.K., ROY J.N., CHATTOPADHYAY T., *A theoretical study of all optical clocked D flip flop using single micro-ring resonator*, Journal of Computational Electronics **13**(1), 2014, pp. 278–286.
[36] ALMEIDA V.R., QIANFAN XU, LIPSON M., *Ultrafast integrated semiconductor optical modulator based on the plasma-dispersion effect*, Optics Letters **30**(18), 2005, pp. 2403–2405.
[37] LI CHUN-FEI, DOU NA, *Optical switching in silicon nanowaveguide ring resonators based on Kerr effect and TPA effect*, Chinese Physics Letters **26**(5), 2009, article 054203.
[38] LAUGHTON F.R., MARSH J.H., ROBERTS J.S., *Intuitive model to include the effect of free carrier absorption in calculating the two-photon absorption coefficient*, Applied Physics Letters **60**(2), 1992, pp. 166–168.
[39] RAKSHIT J.K., ROY J.N., CHATTOPADHYAY T., *Design of micro-ring resonator based all-optical parity generator and checker circuit*, Optics Communications **303**, 2013, pp. 30–37.
[40] RAKSHIT J.K., ROY J.N., CHATTOPADHYAY T., *All-optical XOR/XNOR logic gate using micro-ring resonators*, [In] *5th International Conference on Computers and Devices for Communication (CODEC- 2012)*, IEEE Conference Publications, 2012, pp. 1–4.
[41] LITTLE B.E., FORESI J.S., STEINMEYER G., THOEN E.R., CHU S.T., HAUS H.A., IPPEN E.P., KIMERLING L.C., GREENE W., *Ultra-compact Si-SiO_2 microring resonator optical channel dropping filters*, IEEE Photonics Technology Letters **10**(4) 1998, pp. 549–551.
[42] SARUWATARI M., *All-optical signal processing for terabit/second optical transmission*, IEEE Journal of Selected Topics in Quantum Electronics **6**(6), 2000, pp. 1363–1374.
[43] SHAIK E. H., RANGASWAMY N., *Design of photonic crystal-based all-optical AND gate using T-shaped waveguide*, Journal of Modern Optics **63**(10), 2016, pp. 941–949.
[44] YEN-CHIH LIN, MING-HUA MAO, YOU-RU LIN, HAO-HSIUNG LIN, CHE-AN LIN, LON A. WANG, *All-optical switching in GaAs microdisk resonators by a femtosecond pump–probe technique through tapered-fiber coupling*, Optics Letters **39**(17), 2014, pp. 4998–5001.
[45] YONGHUI TIAN, LEI ZHANG, JIANFENG DING, LIN YANG, *Demonstration of electro-optic half-adder using silicon photonic integrated circuits*, Optics Express **22**(6), 2014, pp. 6958–6965.
[46] YONGHUI TIAN, LEI ZHANG, RUIQIANG JI, LIN YANG, QIANFAN XU, *Demonstration of a directed optical encoder using microring-resonator-based optical switches*, Optics Letters **36**(19), 2011, pp. 3795–3797.
[47] YONGHUI TIAN, LEI ZHANG, RUIQIANG JI, LIN YANG, PING ZHOU, JIANFENG DING, HONGTAO CHEN, WEIWEI ZHU, YANGYANG LU, QING FANG, LIANXI JIA, MINGBIN YU, *Demonstration of a directed optical decoder using two cascaded microring resonators*, Optics Letters **36**(17), 2011, pp. 3314–3316.
[48] LIN YANG, CHUNMING GUO, WEIWEI ZHU, LEI ZHANG, CHANGZHENG SUN, *Demonstration of a directed optical comparator based on two cascaded microring resonators*, IEEE Photonics Technology Letters **27**(8), 2015, pp. 809–812.
[49] ZOIROS K.E., PAPADOPOULOS G., HOUBAVLIS T., KANELLOS G.T., *Theoretical analysis and performance investigation of ultrafast all-optical Boolean XOR gate with semiconductor optical amplifier -assisted Sagnac interferometer*, Optics Communications **258**(2), 2006, pp. 114–134.

[50] HOUBAVLIS T., ZOIROS K.E., KANELLOS G., TSEKREKOS C., *Performance analysis of ultrafast all-optical Boolean XOR gate using semiconductor optical amplifier-based Mach–Zehnder interferometer*, Optics Communications **232**(1–6), 2004, pp. 179–199.

[51] TARAPHDAR C., CHATTOPADHYAY T., ROY J.N., *Mach–Zehnder interferometer based all-optical reversible logic gate*, Optics and Laser Technology **42**(2), 2010, pp. 249–259.

[52] VARDAKAS J.S., ZOIROS K.E., *Performance investigation of all-optical clock recovery circuit based on Fabry–Pérot filter and semiconductor optical amplifier assisted Sagnac switch*, Optical Engineering **46**(8), 2007, article 085005.

[53] RIZOU Z.V., ZOIROS K.E., HATZIEFREMIDIS A., *Semiconductor optical amplifier pattern effect suppression with passive single microring resonator-based notch filter*, Optics Communications **329**, 2014, pp. 206–213.

Received January 14, 2016
in revised form April 4, 2016